

Thermonuclear Burning on the Accreting X-Ray Pulsar GRO J1744-28

Lars Bildsten and Edward F. Brown

Department of Physics and Department of Astronomy

University of California, Berkeley, CA 94720

I: bildsten@fire.berkeley.edu, ebrown@astron.berkeley.edu

Subject headings: accretion – stars: neutron – X-rays: bursts – X-rays: stars

ABSTRACT

We investigate the thermal stability of nuclear burning on the accreting X-ray pulsar GRO J1744-28. The neutron star's dipolar magnetic field is $\lesssim 3 \times 10^{11}$ G if persistent spin-up implies that the magnetospheric radius is less than the co-rotation radius. Bildsten earlier noted that magnetic fields this weak might not quench the vigorous convection sometimes associated with thermonuclear instabilities, so that a convective burning front can propagate around the star in a few seconds and rapidly release the accumulated nuclear energy. After inferring the properties of the neutron star, we study the thermal stability of hydrogen/helium burning and show that thermonuclear instabilities are unlikely causes of the hourly bursts seen at very high accretion rates. We then discuss how the stability of the thermonuclear burning depends on both the global accretion rate and the neutron star's magnetic field strength. We emphasize that the appearance of the instability (i.e., whether it looks like a Type I X-ray burst or a flare lasting a few minutes) will yield crucial information on the neutron star's surface magnetic field and the role of magnetic fields in convection.

We suggest that a thermal instability in the accretion disk is the origin of the long (~ 300 days) outburst and that the recurrence time of these outbursts is > 50 years. We also discuss the nature of the binary and point out that a velocity measurement of the stellar companion (most likely a Roche-lobe filling giant with $m_K \gtrsim 17$) will constrain the neutron star mass.

To Appear in the Astrophysical Journal

1. Introduction

The transient accretion-powered pulsar ($\nu = 2.14$ Hz) GRO J1744-28 was discovered by the Burst and Transient Source Experiment (*BATSE*) aboard the Compton Gamma Ray Observatory (*CGRO*) during a day of rapid bursting (about twenty bursts per hour) on 1995 December 2 (Kouveliotou et al. 1996a; Finger et al. 1996a). Finger et al. (1996a) measured the 11.8 day orbit

and found that GRO J1744-28 was spinning up at a rate $\dot{\nu} = (3.5\text{--}12.2) \times 10^{-12} \text{ s}^{-2}$ between 1995 December 15 and 1996 January 23. The pulsar subsequently settled into a regime of hourly bursting with burst durations of 2–7 seconds, as seen by the PCA instrument on the Rossi X-Ray Timing Explorer (*RXTE*) (Swank 1996; Giles et al. 1996) and the OSSE instrument aboard *CGRO* (Strickman et al. 1996). A qualitatively similar burst has been seen from another accreting pulsar (see our discussion of SMC X-1 in §2), but recurrent bursts of this nature have never been observed.

The bursting behavior has two obvious energy sources: accretion and thermonuclear burning. Lewin et al. (1996) presented the case for accretion-powered bursts via analogy to the Rapid Burster. The rapid bursts (one every few minutes) are responsible for up to 50% of the total time averaged luminosity above 20 keV and thus cannot have a thermonuclear origin (Kouveliotou et al. 1996a). The hourly bursts (over 3000 observed by *BATSE* [Kouveliotou et al. 1996c]) are responsible for a much smaller fraction of the total luminosity, at least above 20 keV. The average burst fluence was $7 \times 10^{-7} \text{ erg cm}^{-2}$ (20–50 keV) on 1996 January 15, when there were 40 per day and the persistent luminosity was 2.5 Crab in the 20–100 keV band (1996 January 16 [Fishman et al. 1996]) and 4.4 ± 0.3 Crab in the 8–20 keV band (1996 January 14–1996 January 15 [Sazonov & Sunyaev 1996]). Above 20 keV, this gives a time-averaged burst luminosity 60–100 times smaller than the steady-state accretion luminosity. The burst energetics below 20 keV (where most of the energy is emitted) is still uncertain due to dead-time corrections in the PCA. Preliminary indications are that these corrections are large enough so that the bursts might be responsible for more than 5% of the < 20 keV emission (Jahoda 1996, private communication).

The burst energies were marginally consistent with nuclear energy release and motivated our theoretical study of thermonuclear burning on this unusual X-ray pulsar. Additional motivations were the matchings of the characteristic decay time (2–10 seconds [Strickman et al. 1996]) with the cooling time at the nuclear burning depth and the mean recurrence time (about 30 minutes for the 260 bursts seen by OSSE from 1996 January 16 to 1996 January 30 [Strickman et al. 1996]) with the time to accumulate enough fuel for an instability. The primary observational evidence against *all* of these bursts having a thermonuclear origin is (1) the independence of the recurrence time from the accretion rate (at least when it is brighter than 200–400 mCrab [Giles et al. 1996]), (2) the existence of “foreshocks” before the bursts (Giles et al. 1996), (3) the lack of spectral evolution during the burst, and (4) the global burst energetics from the PCA instrument (if the dead-time corrections are understood).

We consider here the possibility that this X-ray pulsar has an unusually low field and therefore might exhibit different thermonuclear burning behavior than conventional X-ray pulsars. It is unlikely that the thermonuclear burning was unstable at the peak of the outburst. Hence we concentrate on lower accretion rates, for which the burning will most likely be thermally unstable and will manifest itself as Type I X-ray bursts or flares of a few minutes duration.

Since the presence and character of a thermonuclear instability depends on the neutron star’s magnetic field (B) and global accretion rate (\dot{M}), we begin in §2 by summarizing the indirect

inferences about these quantities. The spin behavior points to an especially weak ($\ll 10^{12}$ G) dipolar magnetic field component and constrains the global accretion rate as well. We also compare GRO J1744-28’s bursting behavior at the peak of the outburst to that of SMC X-1, for which similar arguments point to a low dipole field. In §3, we constrain the binary properties, infer a time-averaged mass transfer rate, and speculate on the origin of the long-term transient behavior. The thermonuclear stability of the accreted hydrogen and helium is discussed in §4 for a range of \dot{M} ’s. Section 5 is a discussion of the magnetic field’s role in the stability and character of nuclear burning in accreting X-ray pulsars. In particular, we discuss in detail how the star will behave as \dot{M} decreases. We conclude, in §6, by describing what a successful identification of a thermonuclear instability implies about the neutron star’s properties.

2. Properties of the Accreting Neutron Star and Comparison to SMC X-1

In addition to the bursting behavior, this pulsar is unusual because of its unusually high spin frequency and its steady spin-up over a large range of accretion rates. In the context of magnetic accretion, these facts imply a dipole field lower than most other accreting pulsars. The magnetosphere is located at $r_m = \xi r_A$ (Ghosh & Lamb 1979), where r_A is a characteristic length found by equating magnetic and fluid stresses, and ξ is a model-dependent dimensionless number. Estimates of ξ range from ≈ 0.52 (Ghosh & Lamb 1979) to ≈ 1 (Arons 1993; Ostriker & Shu 1995; Wang 1995). A measurement of ξ obtained from the observed quasi-periodic oscillations in the accreting pulsar A0535+26 (Finger, Wilson, & Harmon 1996b) gave $\xi \approx 1$. Since the neutron star is spinning up, the magnetospheric radius, r_m , must be less than the co-rotation radius, r_{co} , which implies an *upper* limit on the surface strength of the dipolar component of the magnetic field

$$B \lesssim 3 \times 10^{11} \text{ G } \xi^{-7/4} \left(\frac{\dot{M}}{8 \times 10^{-9} M_{\odot} \text{ yr}^{-1}} \right)^{1/2} \left(\frac{10 \text{ km}}{R} \right)^3, \quad (1)$$

in agreement with previous estimates (Finger et al. 1996a; Sturmer & Dermer 1996). The magnetospheric radius is presently unknown; continual spin-up at lower \dot{M} ’s will reduce this upper limit. This upper bound is less than the typical X-ray pulsar field strength, which, as we discuss in §5, changes the nature of the convection; GRO J1744-28 is the first high accretion rate X-ray pulsar beneath this limit.

The X-ray spectrum above 20 keV falls very steeply (Kouveliotou et al. 1996a; Strickman et al. 1996) and is consistent with being above the characteristic cut-off energy found by *RXTE*/PCA (≈ 15 –20 keV [Swank 1996; Giles et al. 1996]). Daumerie et al. (1996) argue that this spectrum and the increase in pulse fraction with energy imply a surface field $\sim 10^{12}$ G. This argument is at odds with our upper limit on the dipolar component (for $\xi = 1$) and might imply that higher order magnetic moments are present.

We use the measured spin-up rate $\dot{\nu}$ to constrain the accretion rate onto the neutron star. The maximum specific angular momentum of the accreted matter is $l_{\text{max}} \equiv (GM_x r_{co})^{1/2}$, where

$r_{\text{co}} = 1.0 \times 10^8 \text{ cm} \approx 100R$ is the co-rotation radius (where the Kepler frequency equals the neutron star's spin frequency) for a $M_x = 1.4M_\odot$ neutron star. Because the observed torque $2\pi I\dot{\nu}$ must be less than $\dot{M}l_{\text{max}}$ (Ghosh & Lamb 1979; Chakrabarty et al. 1993), we set a lower bound to \dot{M} ,

$$\dot{M} > 8 \times 10^{-9} M_\odot \text{ yr}^{-1} \left(\frac{\dot{\nu}}{10^{-11} \text{ s}^{-2}} \right) \left(\frac{R}{10 \text{ km}} \right)^2, \quad (2)$$

where $I = 0.4M_x R^2$ is the neutron star's moment of inertia (a good approximation for our choice of mass and radius [Ravenhall & Pethick 1994]). The spherically averaged local accretion rate,

$$\dot{m}_{\text{sph}} \equiv \frac{\dot{M}}{4\pi R^2} > 4 \times 10^4 \text{ g cm}^{-2} \text{ s}^{-1} \left(\frac{\dot{\nu}}{10^{-11} \text{ s}^{-2}} \right), \quad (3)$$

is then *independent* of the neutron star's radius. Using a rough bolometric flux for 1996 January 15 of $10^{-7} \text{ erg cm}^{-2} \text{ s}^{-1}$, we infer a minimum distance $d = 3 \text{ kpc}$. As we note later, the extinction and position in the galaxy most likely place the object at least 8 kpc away.

The only other accreting pulsar which has always been spinning up ($\dot{\nu} = 2.4 \times 10^{-11} \text{ s}^{-2}$) and for which our earlier arguments yield a comparable field strength is SMC X-1 ($\nu = 1.4 \text{ Hz}$). For a typical accretion rate $\dot{M} \approx 4 \times 10^{-8} M_\odot \text{ yr}^{-1}$ (Levine et al. 1993), we infer $B < 10^{12} \text{ G}$. Angelini, Stella, and White (1991) discovered an X-ray burst from SMC X-1 during an *EXOSAT* observation on 18 October 1984 when the 1-16 keV luminosity was $L \approx 4 \times 10^{38} \text{ erg s}^{-1}$. This burst is *very* similar to the large hourly bursts seen from GRO J1744-28. The burst rose by a factor of three within one second, lasted for about 80 seconds, and was followed by a 35% decline in the persistent flux. There was no evidence for spectral changes during or after the burst, and the pulse fraction and phase remained constant. The recurrence time must be long, as only one burst was seen in ≈ 20 hours of observation. Angelini et al. (1991) noted the similarities to the Rapid Burster and argued for accretion as the energy source for these events. They also noted that the variability of the source has a strong underlying quasi-period of a few minutes, which was present in all *EXOSAT* observations except for the five hours following the burst. About 10% of the total luminosity of the source is in these variations.

3. Properties of the Binary

Following the *ROSAT* positioning of this object (Kouveliotou et al. 1996b), Augusteijn et al. (1996) identified the variable infra-red counterpart, which was present in an earlier image (8 February 1996) of Blanco, Lidman, and Glazebrook (1996) at $m_K = 15.7 \pm 0.3$ and was undetected and at least a magnitude fainter on 28 March 1996. This light is most likely X-rays reprocessed by either the accretion disk or companion (Augusteijn et al. 1996). The most obvious Roche-lobe filling object is a first-ascent red giant branch star with a degenerate helium core of mass M_{He} and an overlying hydrogen envelope (Finger et al. 1996a; Sturmer & Dermer 1996). Hydrogen shell burning via the CNO cycle supplies a luminosity strongly dependent on only the helium core mass,

which allows us to estimate the stellar luminosity and expected IR magnitude. In the absence of mass or angular momentum loss, this binary evolves due to the expansion of the red giant as the helium core mass grows.

3.1. Constraints on the Optical Companion and Neutron Star Mass

We solve for the companion mass, M_c , by using the orbital parameters $P_{\text{orb}} = 11.83$ d and $a_x \sin i = 2.63$ lt-sec (Finger et al. 1996a) and the core-mass/luminosity relations of Webbink, Rappaport, & Savonije (1983). We presume that the giant fills the Roche lobe estimated by Eggleton (1983) and fix $M_x = 1.4M_\odot$. For metallicities $Z = 0.02(0.0001)$, the first allowed solution (corresponding to an unrealistic hydrogen envelope mass of zero) has $M_c/M_\odot = 0.216(0.232)$ and inclinations less than 18–19 degrees ($\cos i > 0.95$). The solution in the middle of the allowed range (i.e., $\cos i = 0.975$) has $M_c = 0.334 M_\odot$, $M_{\text{He}} = 0.22(0.24)M_\odot$, $L \approx 12L_\odot$, an orbital separation of $26R_\odot$, a stellar radius of $6.9R_\odot$, and a projected companion velocity $K \approx 20 \text{ km s}^{-1}$. The helium core mass is slightly larger for the metal-poor case to compensate for fewer catalysts. The strong dependence of the giant radius on M_{He} makes the inferred core mass (shown by the dotted line in Figure 1) nearly independent of the inclination angle and always close to $0.22(0.24)M_\odot$. The dashed line in Figure 1 shows M_c as a function of $\cos i$ for $Z = 0.02$ and $M_x = 1.4M_\odot$. The resulting mass transfer rate (Webbink et al. 1983) is given by the solid line in Figure 1. For the “typical” solution presented above, the average mass transfer rate is $\dot{M} \approx 10^{-9}M_\odot \text{ yr}^{-1}$, and the hydrogen envelope mass is $0.1M_\odot$. This implies a lifetime, nearly independent of the metallicity, of 10^8 yr. Most of the giant’s envelope goes onto the neutron star (for conservative evolution).

Unless we are looking at the system nearly pole-on, we must conclude that $M_c \approx 0.3M_\odot$. If this low-mass star followed a normal evolutionary track, then it must have started mass transfer as a $\approx M_\odot$ star. If all the departed mass accreted onto the compact object, then either the neutron star is more massive than its “birthweight” ($1.2\text{--}1.7M_\odot$ [Timmes, Woosley, & Weaver 1996]), or the neutron star was a white dwarf that underwent accretion-induced collapse. Considering more massive neutron stars does not alleviate the companion’s substantial mass loss but does increase the inclination angle (e.g., $\cos i = 0.9$ for $M_x = 2.0M_\odot$, a doubling of the allowed phase space).

Depending on the inclination angle, an infrared measurement of the orbit of this system might actually constrain the neutron star mass. The projected companion velocity is

$$K = \left(\frac{2\pi a_x \sin i}{P_{\text{orb}}} \right) \left(\frac{M_x}{M_c} \right) = 4.85 \text{ km s}^{-1} \left(\frac{M_x}{M_c} \right). \quad (4)$$

We find the minimum companion mass by requiring (1) that the star be luminous enough so that it fills the Roche lobe, and (2) that the overlying hydrogen envelope have a minimum mass of $10^{-2}M_\odot$ so as to live for at least 10^7 yr and to be fully convective. The minimum companion mass ($M_c = 0.22M_\odot$) is then basically independent of M_x , so that the maximum K for the Roche-lobe filling giant hypothesis is $K_{\text{max}} = 21 \text{ km s}^{-1}(M_x/M_\odot)$. Hence, a measurement of K can potentially

constrain the neutron star mass. For example, if $M_x = 2M_\odot$ and we presume that $\cos i$ is uniformly distributed between 0.9 and 1.0, then there is a 50% chance of measuring a velocity larger than the maximum for the $1.4M_\odot$ neutron star case. This will be a tough job. We find that the stellar effective temperature is in the range 4000–4200 K, which, for the luminosity derived above, gives $M_K \approx -0.2$ (Bessell & Brett 1988). If the extinction is $A_V \approx 25$, as implied by the $N_H \approx (5-6) \times 10^{22} \text{ cm}^{-2}$ measurement of Dotani et al. (1996), then $A_K \approx 3$ and for a distance of 8 kpc, we expect $m_K \approx 17$.

3.2. The Long-Term Accretion History

Consistent with the transient nature of this binary, the inferred long-term mass transfer rate is less than the current accretion rate. This possibly indicates that the present outburst (which so far has lasted for over 300 days) arises from a thermal instability in the accretion disk similar to that occurring in dwarf novae. Indeed, the implied long term mass transfer rate is much less than the amount needed for stable mass transfer (Shafter 1992). Our orbital calculations give the distance from the neutron star to where the accreting matter strikes the accretion disk as $R_r \approx 4R_\odot$ (Lubow & Shu 1975). The thermal instability occurs when the column density of matter (Σ) accumulated at this radius exceeds $\gtrsim 10^3 \text{ g cm}^{-2}$ (Cannizzo & Wheeler 1984), in which case the accumulated mass is $\gtrsim R_r^2 \Sigma \sim 5 \times 10^{-8} M_\odot$. This requires over 50 years of mass transfer from the giant and supplies more than enough material to power the large outburst.

The accretion will most likely be halted by a propeller effect at low accretion rates (Illarionov & Sunyaev 1975). However, even when not accreting, the neutron star has a luminosity from the cooling core (at temperature T_c) given by Gudmundsson, Pethick, and Epstein (1983) as

$$L_{\text{core}} = 6 \times 10^{32} \text{ erg s}^{-1} \left(\frac{M_x}{1.4M_\odot} \right) \left(\frac{T_c}{10^8 \text{ K}} \right)^{2.2}. \quad (5)$$

This luminosity will probably not quench the thermal instability of the accretion disk as fully exposed matter at R_r only has an effective temperature of $T_{\text{eff}} = 1800 \text{ K} (T_c/10^8 \text{ K})^{0.55}$. It is the unusual combination of large orbital separation, low inferred mass transfer rates, and low neutron star luminosity that allows for such instabilities in this neutron star binary. For time-averaged accretion rates $\approx 10^{-9} M_\odot \text{ yr}^{-1}$, the outburst intervals are longer than the history of X-ray and γ -ray monitoring. The system’s extinction ($A_V > 25$) also makes optical identification of a prior outburst unlikely.

4. The Nuclear Burning of Accreted Matter

The thermal stability and appearance of nuclear burning on steadily accreting neutron stars is well studied. For comparable metallicities and magnetic fields weak enough so as not to affect the opacities ($< 10^{13} \text{ G}$), the only residual difference between this neutron star and others accreting at

comparable local rates is a colder core. This might allow for unstable hydrogen/helium ignition at slightly higher instantaneous local accretion rates (\dot{m}) than on a steadily accreting star.

Constant accretion at these \dot{M} 's conductively heats the neutron star core, which attains an equilibrium temperature of $T_c = (2-4) \times 10^8$ K in about 10^3-10^4 yr by balancing this heating with neutrino cooling (Ayasli & Joss 1982). The time-averaged \dot{M} in GRO J1744-28 is comparable to many X-ray binaries, whereas the instantaneous \dot{M} can clearly be much higher. The cycling of \dot{M} leads to a colder equilibrium core than that of a neutron star steadily accreting at the same time-averaged \dot{M} . This is because the thermal timescale of the deep ocean and crust (which is where substantial energy release occurs as matter is forced through the electron capture boundaries [Haensel & Zdunik 1990]) is $\sim 10-100$ years, much longer than the outburst duration. There is thus insufficient time to heat the crust to a temperature profile favorable for sending a large luminosity $L \approx (\dot{M}/m_p)(1 \text{ MeV})$ into the core. In addition, between outbursts, the cold outer envelope conducts away the accumulated heat in the deep ocean and crust. For temperatures below $T_c \sim 2 \times 10^8$ K the core cools radiatively between outbursts, much as a young neutron star still hot from birth.

4.1. Settling and Nuclear Burning of the Accreting Matter

As described in §3, the neutron star is accreting the hydrogen-rich envelope of an evolved giant. Because the giant has already lost an appreciable amount of mass, the matter presently being transferred was most likely processed in the companion's interior during its main sequence lifetime. This would increase the helium content. The β -decay limitations and high temperatures on the neutron star fix the hydrogen burning (via the CNO cycle) rate at the β -decay limited value of the "hot" CNO cycle, $\epsilon_H = 5.8 \times 10^{15} Z_{\text{CNO}} \text{ erg g}^{-1} \text{ s}^{-1}$ where Z_{CNO} is the mass fraction of the CNO elements. For high accretion rates, this burning never consumes the accreted hydrogen before helium ignition, so that unstable helium burning occurs in a hydrogen-rich environment, which enhances the nuclear reaction chains and energy release (Lamb & Lamb 1978; Taam & Picklum 1979; Fujimoto et al. 1981; Taam 1982). Because of the complicated rp process (Wallace & Woosley 1981), the exact composition of the ashes is unknown except for a few limited cases (Van Wormer et al. 1994).

Prior to helium ignition, the accreted material is settling onto the neutron star and is stably burning hydrogen. Since the thermal time is always less than the time to accrete to a given depth, $t_{\text{accr}} = y/\dot{m}$, we find the temperature structure by solving the time-independent entropy and flux equations,

$$T\dot{m}\frac{ds}{dy} = \frac{dF}{dy} + \epsilon_H, \quad F = \frac{c}{3\kappa} \frac{daT^4}{dy}, \quad (6)$$

where the local accretion rate is written as $\dot{m} = \dot{m}_4 10^4 \text{ g cm}^{-2} \text{ s}^{-1}$, s is the specific entropy, F is the outward heat flux, and y is the column depth. The opacity in the upper atmosphere is given by $1/\kappa = 1/\kappa_{\text{rad}} + 1/\kappa_{\text{cond}}$, where the radiative opacity is the sum of electron scattering (we

use Paczyński’s [1983] fitting formulae for the degeneracy and high temperature corrections) and free-free absorption. We use the conductivity from Yakovlev & Urpin (1980).

These settling solutions are valid until the helium burns fast enough to appreciably change either the temperature or the helium abundance. Fushiki and Lamb (1987) defined the boundary of stable helium burning in the y - T plane (the ignition curve) by setting

$$\frac{d\epsilon_{3\alpha}}{dT} = \frac{d\epsilon_c}{dT}, \quad (7)$$

where $\epsilon_c = acT^4/3\kappa y^2$ is a local representation of the conductive cooling and $\epsilon_{3\alpha}$ is the helium burning rate. These derivatives are taken at constant pressure, as the instability grows faster than the pressure changes. The heavy dot-dashed line in Figure 2 denotes this ignition curve for $Y = 0.3$. Regions to the right of this curve are thermally unstable to helium burning. We also define the depletion curve by equating the helium lifetime to the 3α reaction with t_{accr} (Fushiki & Lamb 1987); the heavy solid lines in Figure 2 denote this condition for $\dot{m}_4 = 3, 7.5,$ and 30 .

We derive the settling solutions by varying the flux exiting the atmosphere until the flux is zero at the depth where the ignition curve (or depletion curve, whichever is first) is met. We take zero flux at the bottom to mimic the cold core. These settling solutions all strike the ignition curve before the depletion curve, so that we find the column density y_{ign} accumulated on the star prior to unstable helium ignition.

For Population I type metallicities, the temperature of the settling material is mostly set by the slight amount of hydrogen burning. Indeed, as is evident in the three light solid lines that display these settling solutions in Figure 2, y_{ign} depends only mildly on \dot{m} for the $Z_{\text{CNO}} = 0.01$ case. We obtain $y_{\text{ign}}/10^8 \text{ g cm}^{-2} = 3.1, 2.95,$ and 2.65 for $\dot{m}_4 = 3, 7.5,$ and 30 ; these correspond to recurrence times of 2.9 hours, 1.1 hours, and 15 minutes. The flux exiting the atmosphere is $F/(10^{22} \text{ erg cm}^{-2} \text{ s}^{-1}) = 2.0, 2.42,$ and 4.93 for these \dot{m} ’s.

Lower CNO abundances are relevant if the companion is an older Population II giant and/or if spallation of the incident nuclei occurs in the accretion shock (Bildsten, Salpeter, & Wasserman 1992). At lower Z_{CNO} , the settling solutions are more sensitive to the accretion rate via the gravitational compression terms. The two bottom thin solid lines in Figure 2 are settling solutions when $Z_{\text{CNO}} = 10^{-4}$ for $\dot{m}_4 = 7.5$ and 30 , giving recurrence times of 6.6 hours and 0.5 hours.

4.2. When is the Burning Time Dependent?

The crucial question to answer is, “At what accretion rate is the burning unstable?”. The simplest way to address this is to construct the steady-state solution (represented by the dotted lines in Figure 2 for the \dot{m} ’s given above) that burns the material as fast as it accretes. If this solution does not consume the fuel before reaching the instability curve, then it is unstable. For an accretion rate below $\dot{m}_{\text{crit}} \approx 3 \times 10^4 \text{ g cm}^{-2} \text{ s}^{-1}$, the burning is unstable (for $Y = 0.3$). This critical

accretion rate increases by a factor of two if the helium mass fraction is 0.5. These estimates also indicate that the burning is stable when $\dot{m} > \dot{m}_{\text{crit}}$.¹ Since \dot{m}_{crit} is smaller than our minimum estimated accretion rate at the outburst peak, it is unlikely that the hourly bursts during the brightest parts of the outburst have a thermonuclear origin.

However, the burning becomes unstable when $\dot{m} < \dot{m}_{\text{crit}}$ (either due to a reduction in the overall accretion rate or spreading away from the polar cap; see §5). When the fuel spreads over the whole star prior to ignition, the maximum luminosity (and hence flux) at which an instability occurs is $L \approx 7 \times 10^{37} \text{ erg s}^{-1}$ (for $\dot{m}_{\text{crit}} = 3 \times 10^4 \text{ g cm}^{-2} \text{ s}^{-1}$ and $R = 10 \text{ km}$). This corresponds to a bolometric flux

$$F_{\text{unstable}} < 10^{-8} \text{ erg cm}^{-2} \text{ s}^{-1} \left(\frac{L}{7 \times 10^{37} \text{ erg s}^{-1}} \right) \left(\frac{8 \text{ kpc}}{d} \right)^2. \quad (8)$$

We convert this to cs^{-1} in the PCA instrument aboard *RXTE* by using the conversion factor (Giles et al. 1996) of $4 \times 10^{-8} \text{ erg cm}^{-2} \text{ s}^{-1}$ (2–60 keV) for 10^4 cs^{-1} . For $d = 8 \text{ kpc}$, unstable burning signatures will most likely not appear until the PCA count rate is $\lesssim 2500 \text{ cs}^{-1}$.

When the burning is unstable, the intersection of the settling solutions with the helium ignition curve defines y_{ign} . For typical metallicities, $y_{\text{ign}} > 1.5 \times 10^8 \text{ g cm}^{-2}$, which at \dot{m}_{crit} gives a recurrence time of just over an hour. Once the helium ignites, the temperature rises rapidly and starts a propagating combustion front. If the whole star is ignited (see next section) the maximum burst energy would be $4\pi R^2 y_{\text{ign}} (7 \text{ MeV}/m_p)$. This is the maximum, as time-dependent calculations of the hydrogen/helium burning flash often found incomplete burning (Taam et al. 1993) and the whole star need not ignite. The resulting fluence would be

$$\text{Maximum Burst Fluence} = 1.5 \times 10^{-6} \text{ erg cm}^{-2} \left(\frac{y_{\text{ign}}}{1.5 \times 10^8 \text{ g cm}^{-2}} \right) \left(\frac{R}{10 \text{ km}} \right)^2 \left(\frac{8 \text{ kpc}}{d} \right)^2. \quad (9)$$

The peak luminosity depends on the combustion front’s propagation speed through the fuel-rich regions, as we now discuss.

5. The Role of the Magnetic Field

Conventional Type I X-ray bursts are not seen from highly magnetized ($B \gtrsim 10^{12} \text{ G}$) accreting X-ray pulsars. This was at first surprising because they accrete at rates comparable to X-ray burst sources that are not obviously magnetic. Joss and Li (1980) explained the lack of bursts

¹There have been indications in the past that the \dot{m}_{crit} obtained from a time dependent simulation might actually be higher than our estimate. In particular, Ayasli and Joss (1982) argued that the steady state solution would not be reached until the time to reach the ignition depth became shorter than the local thermal time. This requires accretion rates 2–5 times higher than our estimate. However, in the absence of a full time-dependent calculation, we will stick to our present, and maybe overly conservative, estimate.

by *stabilizing* the nuclear burning with two mechanisms. For this pulsar, the relevant mechanism is the increased local accretion rate on the polar cap. The magnetic field funnels the accretion onto the polar cap and confines the accretion mound until the ignition pressure is reached. These constraints are typically satisfied for steadily accreting X-ray pulsars with $\dot{M} \gtrsim 10^{-10} M_{\odot} \text{ yr}^{-1}$, as the fractional area of the polar cap only needs to satisfy $A_{\text{cap}}/4\pi R^2 \lesssim 0.01$. This is well within the estimates obtained by either following the field lines from the magnetospheric radius to the star (Lamb, Pethick, & Pines 1973),

$$A_{\text{cap}} \approx 10^{11} \text{ cm}^2 \xi^{-1} \left(\frac{B}{10^{11} \text{ G}} \right)^{-4/7} \left(\frac{\dot{M}}{10^{-8} M_{\odot} \text{ yr}^{-1}} \right)^{2/7} \left(\frac{R}{10 \text{ km}} \right)^{9/7}, \quad (10)$$

or allowing the matter to penetrate through the magnetopause via a Rayleigh-Taylor instability and attach to field lines at smaller radii (Arons & Lea 1976; Elsner & Lamb 1977).

The absence of Type I X-ray bursts in *all* X-ray pulsars seems unlikely given the range in magnetic field strengths and accretion rates. Bildsten (1995) suggested that, even when the burning is thermally unstable, a strong magnetic field will inhibit the rapid lateral convective motion needed for the combustion front to ignite the whole star in a few seconds (Fryxell & Woosley 1982). The field strength required to halt the convective ($\sim 10^6 \text{ cm s}^{-1}$) propagation of burning fronts is not known. Convection is potentially stabilized when $B^2 > 8\pi P$ (Gough & Tayler 1966), which requires $B \gtrsim 7 \times 10^{11} \text{ G}$ in the helium burning region.² Most inferred dipolar field strengths for accreting X-ray pulsars easily satisfy this constraint. However, GRO J1744-28 does not and hence is an especially intriguing candidate for showing Type I X-ray bursts.

If the lateral convective motion is inhibited (or if there is too little fuel for convection to occur [Bildsten 1993]) then the burning front propagates at the slower speed set by heat transport (electron conduction and/or radiative transport, depending on the depth)

$$v_{\text{slow}} \approx 80 + 200 \left(\frac{y_{\text{He}} - y_q}{4.5 \times 10^7 \text{ g cm}^{-2}} \right) \text{ cm s}^{-1}, \quad (11)$$

where y_{He} is the local helium column density (in g cm^{-2}) and $y_q = 1.35 \times 10^8 \text{ g cm}^{-2}$ is the minimum column density needed for a pure helium burning front to propagate (Bildsten 1995). This relation is for a pure helium atmosphere and is a reasonable lower limit to the mixed hydrogen/helium burning case. For the typical $y_{\text{He}} \approx 2 \times 10^8 \text{ g cm}^{-2}$ where the instability sets in, $v_{\text{slow}} \approx 400 \text{ cm s}^{-1}$, so that the burning front crosses a 10^5 cm polar cap in $t_{\text{cross}} \approx 4 \text{ min}$. In this case, the thermonuclear instability would appear as a flare of a few minutes duration (potentially time symmetric) with a luminosity set by the amount of accumulated fuel and the time to burn all of it, $L_{\text{flare}} \approx 0.05 L_{\text{accr}} (t_{\text{accr}}/t_{\text{cross}})$ (Bildsten 1995).

² Even lower fields might slow the burning fronts, as the sub-sonic velocities ($v_c \sim 10^6 \text{ cm s}^{-1}$) implied by efficient convection can only push around fields of strength $B^2 < 8\pi\rho v_c^2$, or $B < 10^9 \text{ G}$ at the helium ignition depth (Bildsten 1995). Observations will most likely tell us the outcome for magnetic fields in the intriguing regime $\rho v_c^2 \ll B^2/8\pi \ll P$ ($10^9 \text{ G} < B < 7 \times 10^{11} \text{ G}$).

5.1. The Spreading of Accreted Fuel

The local accretion rate, \dot{m} , onto the polar cap would greatly exceed \dot{m}_{sph} if accretion onto GRO J1744-28 is via a polar cap of the size given by equation (10) (this is not clear given the small pulse fraction and nearly sinusoidal pulses seen by Finger et al. [1996a]). Because the fate of the accreted material depends on \dot{m} , knowing the depth at which accreted matter flows laterally over the surface and reduces \dot{m} to \dot{m}_{sph} is crucial. The magnetic Reynolds number of the flow is $4\pi\sigma\ell v/c^2$, where ℓ is the length over which the magnetic field varies, σ is the electrical conductivity, and $v = \dot{m}/\rho$ is the downward flow velocity. Using the pressure scale height, $h = P/\rho g$, as an estimate for ℓ , we find that the magnetic Reynolds number is ~ 100 in the helium burning region ($P \approx 10^{22} \text{ erg cm}^{-3}$, $T \approx 5 \times 10^8 \text{ K}$). As a result, the magnetic field is frozen into the matter at the ignition depth.

For a small polar cap, we find the pressure where the magnetic field can no longer hold up the accretion mound by balancing the transverse pressure gradient (given by the lateral extent of the polar cap, $\ell_{\text{cap}} \sim \sqrt{A_{\text{cap}}} < R$) with a distorted field. Following Hameury et al. (1983), we presume spreading occurs at the depth where the field is distorted by a large angle. To illustrate this problem, consider an azimuthally symmetrical and poloidal magnetic field $\mathbf{B} = (B_{\varpi}, 0, B_z)$ in cylindrical coordinates (ϖ, ϕ, z) . The characteristic length in the z -direction is the pressure scale height $h = P/\rho g$ and the characteristic length in the ϖ -direction is ℓ_{cap} . The accretion flow distorts the field from $\mathbf{B} = (0, 0, B)$ to the perturbed configuration $\mathbf{B} = (B_{\varpi}, 0, B - \delta B_z)$. Equating estimates of \mathbf{J} obtained from $\text{curl } \mathbf{B} = 4\pi\mathbf{J}/c$ and the ϖ -component of $-\nabla P + \rho\mathbf{g} + \mathbf{J} \times \mathbf{B}/c = \mathbf{0}$, and using $\text{div } \mathbf{B} = 0$ to obtain a relation between δB_z and B_{ϖ} , we have

$$\frac{B_{\varpi}}{B} \sim \frac{4\pi h P}{\ell_{\text{cap}} B^2}. \quad (12)$$

For a fully ionized H/He mixture with an ideal gas equation of state, the pressure where $B_{\varpi} \sim B$ is

$$P_{\text{spread}} \sim 10^{22} \text{ erg cm}^{-3} \left(\frac{A_{\text{cap}}}{10^{11} \text{ cm}^2} \right)^{1/2} \left(\frac{B}{10^{10} \text{ G}} \right)^2 \left(\frac{2 \times 10^8 \text{ K}}{T} \right). \quad (13)$$

This pressure defines a boundary (y_s in column depth) where the matter starts to spread laterally. We will presume that above y_s the local accretion rate is \dot{M}/A_{cap} and that below y_s , the local accretion rate is the spherical value \dot{m}_{sph} .

5.2. Global Behavior of the Nuclear Burning for GRO J1744-28

Having shown that the nuclear burning is unstable when $\dot{m} < \dot{m}_{\text{crit}} \approx 3 \times 10^4 \text{ g cm}^{-2} \text{ s}^{-1}$, we now estimate \dot{m} at the ignition depth in terms of the dipole magnetic moment μ and global accretion rate \dot{M} (we are assuming for simplicity that no higher-order multipole moments are present). We show in Figure 3 the cases $\xi = 1.0$ and $\xi = 0.5$. Within this parameter space, the first requirement is that the magnetospheric radius be less than the co-rotation radius (eq. [1] with R set to 10 km)

and is indicated by the unhatched area. The second relation, indicated by the dot-dashed line in Figure 3, is $y_s = y_{\text{ign}}$. Below this line, the accretion flow spreads before ignition, thereby lowering the local accretion rate to \dot{m}_{sph} . Depending on the dipolar field strength there are two cases.

- For $B \lesssim (2-4) \times 10^{10}$ G, the accreted matter spreads before igniting regardless of the polar cap area. Thus, the relevant local accretion rate (indicated by the vertical dashed line) is \dot{m}_{sph} and the burning is unstable when the flux constraint (eq. [8]) is reached. This case is denoted by region I in Figure 3.
- For $B \gtrsim (2-4) \times 10^{10}$ G, the matter ignites prior to spreading, so that the nature of the thermonuclear burning depends on the polar cap size. This case is denoted by region II in Figure 3. The most constraining polar cap area is given by equation 10 and is indicated by the slanted dotted line in the right-hand plot. For GRO J1744-28, this scenario is only relevant if $\xi \sim 0.5$, as otherwise the propeller effect will halt accretion before $\dot{m} < \dot{m}_{\text{crit}}$ on the polar cap. For $\xi = 1.0$, nuclear burning in region II is unstable only if the polar cap area is larger than the estimate of equation (10).

Our ignorance of the polar cap size prohibits us from saying at what accretion rate the $B \gtrsim (2-4) \times 10^{10}$ G case becomes unstable (the triangular regions denoted II). If we choose a fixed polar cap area of 10% of the stellar area, then the \dot{M} needed for an instability decreases by a factor of ten, as does the maximum flux required to see an instability. The polar cap of Arons and Lea (1980) is always larger than 10% of the stellar area and implies that the burning becomes unstable when $L < 3 \times 10^{37}$ erg s⁻¹. The appearance of unstable burning will constrain the polar cap size, as a necessary condition for stable burning is $A_{\text{cap}} < \dot{M}/\dot{m}_{\text{crit}}$.

6. Summary and Observational Outlook

The continuous monitoring of GRO J1744-28 by the *RXTE* provides an important opportunity to learn about both accretion and thermonuclear instabilities on a weakly magnetized neutron star. We have shown that the bursts observed during the peak of the outburst are most likely not of thermonuclear origin, as even the minimum local accretion rate on the neutron star is too high for unstable burning of hydrogen-rich material. This statement is no longer true as the accretion rate, \dot{M} , decreases.

The full understanding of the thermonuclear burning depends on many properties of both the neutron star and the binary. In §2, we used the observed torque to estimate the minimum accretion rate and dipole field, which led to the comparison with SMC X-1, another bursting X-ray pulsar. We speculated in §3.2 that the present outburst might be the result of a thermal instability in the disk, comparable to what occurs in dwarf novae. We also discussed the optical companion and pointed out that a careful velocity measurement of the companion will constrain the neutron star mass.

We have shown that, if $B \lesssim (2-4) \times 10^{10}$ G, then the nuclear burning becomes unstable when the intrinsic source luminosity is $L \lesssim 7 \times 10^{37}$ erg s $^{-1}$. For higher magnetic fields, the matter stays confined at the polar cap before ignition, in which case the stability of the nuclear burning depends strongly on the polar cap size. As the outburst fades and \dot{M} decreases, the burning might become unstable, especially if the polar cap is larger than the conventional estimate (equation [10]), for which the thermonuclear burning is always stable when $\xi = 1$. Hence, for larger fields, the global accretion rate when the first signatures of thermonuclear instability appear will constrain the polar cap size.

As discussed in §5, the character of the instability strongly depends on the burning front’s propagation speed. If the instability is too weak to convect (or if the field is strong enough, $B \gtrsim 7 \times 10^{11}$ G, to inhibit the lateral convective heat transport) a possible burning signature is flares with durations of a few minutes to an hour. The duration of the flare is set by the slow burning speed (§5) and the size of the fuel-rich region. These flares rise on a timescale comparable to their duration and are not necessarily asymmetrical in time, as Type I X-ray bursts are. For a polar cap radius of 10^5 cm (10% of the stellar radius) and a typical ignition depth of 2×10^8 g cm $^{-2}$, the burning front crosses the polar cap in four minutes. If convection occurs, then we expect to see Type I X-ray bursts as in other Low Mass X-Ray Binaries.

When bursts or flares first appear, they will have recurrence times of order an hour if our \dot{m}_{crit} determination is accurate. It is possible that the recurrence times will be longer than this (especially for low metallicity), in which case detection will be more difficult. The ability of the PCA to position bursts to within 0.2 degrees has already eliminated GRO J1744-28 as the source of two Type I X-ray bursts seen in the field (Corbet & Jahoda 1996; Jahoda et al. 1996) and should eventually provide an unambiguous localization of a Type I burst from GRO J1744-28.

We thank Jon Arons, Mark Finger, Keith Jahoda, Chris McKee, Ed Morgan, Tom Prince and Bob Rutledge for many discussions about the nature of this source. We especially thank Bob Rutledge (MIT) for creating and maintaining a Web site about this X-ray binary. Our work was supported by NASA via grants NAG 5-2819 and NAGW-4517 and by the California Space Institute (CS-24-95). L. B. was also supported by the Alfred P. Sloan Foundation.

REFERENCES

- Angelini, L., Stella, L., & White, N. E. 1991, ApJ, 371, 332
- Arons, J., & Lea, S. M. 1976, ApJ, 207, 914
- Arons, J., & Lea, S. M. 1980, ApJ, 235, 1016
- Arons, J. 1993, ApJ, 408, 160
- Augusteijn, T., et al. 1996, IAU Circ., 6369

- Ayasli, S., & Joss, P. C. 1982, *ApJ*, 256, 637
- Bessell, M. S., & Brett, J. M. 1988, *PASP*, 100, 1134
- Bildsten, L. 1993, *ApJ*, 418, L21
- Bildsten, L. 1995, *ApJ*, 438, 852
- Bildsten, L., Salpeter, E. E., & Wasserman, I. 1992, *ApJ*, 384, 143
- Blanco, P., Lidman, C., & Glazebrook, K. 1996, *IAU Circ.*, 6321
- Cannizzo, J. K., & Wheeler, J. C. 1984, *ApJS*, 55, 367
- Chakrabarty, D., et al. 1993, *ApJ*, 403, L33
- Corbet, R., & Jahoda, K. 1996, *IAU Circ.*, 6399
- Daumerie, P., Kalogera, V., Lamb, F. K., & Psaltis, D. 1996, *Nature*, 382, 141
- Dotani, T., Ueda, Y., Ishida, M., Nagase, F., & Inoue, H. 1996, *IAU Circ.*, 6337
- Eggleton, P. P. 1983, *ApJ*, 268, 368
- Elsner, R. F., & Lamb, F. K. 1977, *ApJ*, 215, 897
- Finger, M. H., Koh, D. T., Nelson, R. W., Prince, T. A., Vaughan, B. A., & Wilson, R. B. 1996a, *Nature*, 381, 291
- Finger, M. H., Wilson, R. B., & Harmon, B. A. 1996b, *ApJ*, 459, 288
- Fishman, G. J., et al. 1996, *IAU Circ.*, 6290
- Fryxell, B. A., & Woosley, S. E. 1982, *ApJ*, 261, 332
- Fujimoto, M. Y., Hanawa, T., & Miyaji, S. 1981, *ApJ*, 246, 267
- Fushiki, I., & Lamb, D. Q. 1987, *ApJ*, 323, L55
- Ghosh, P., & Lamb, F. K. 1979, *ApJ*, 234, 296
- Giles, A. B., Swank, J. H., Jahoda, K., Zhang, W., Strohmayer, T., Stark, M. J., & Morgan, E. H. 1996, *ApJ*, 469, L25
- Gough, D. O., & Tayler, R. J. 1966, *MNRAS*, 133, 85
- Gudmundsson, E. H., Pethick, C. J., & Epstein, R. I. 1983, *ApJ*, 272, 286
- Haensel, P., & Zdunik, J. L. 1990, *A&A*, 227, 431

- Hameury, J. M., Bonazzola, S., Heyvaerts, J., & Lasota, J. P. 1983, *A&A*, 128, 369
- Illarionov, A. F. & Sunyaev, R. A. 1975, *A&A*, 39, 185
- Jahoda, K., Swank, J. H., Giles, A. B., Stark, M. J., Strohmayer, T., Zhang, W., & Morgan, E. H. 1996, submitted to *Proc. SPIE 2808, EUV, X-Ray, and Gamma Ray Instrumentation for Astronomy VII*
- Joss, P. C., & Li, F. K. 1980, *ApJ*, 238, 287
- Kouveliotou, C., van Paradijs, J., Fishman, G. J., Briggs, M. S., Kommers, J., Harmon, B. A., Meegan, C. A., & Lewin, W. H. G. 1996a, *Nature*, 379, 799
- Kouveliotou, C., et al. 1996b, *IAU Circ.*, 6369
- Kouveliotou, C., et al. 1996c, *IAU Circ.*, 6395
- Lamb, D. Q., & Lamb, F. K. 1978, *ApJ*, 220, 291
- Lamb, F. K., Pethick, C. J., & Pines, D. 1973, *ApJ*, 184, 271
- Levine, A., Rappaport, S., Deeter, J. E., Boynton, P. E., & Nagase, F. 1993, *ApJ*, 410, 328.
- Lewin, W. H. G., Rutledge, R. E., Kommers, J. M., van Paradijs, J., & Kouveliotou, C. 1996, *ApJ*, 462, L39
- Lubow, S. H., & Shu, F. H. 1975, *ApJ*, 198, 383
- Ostriker, E. C., & Shu, F. H. 1995, *ApJ*, 447, 813
- Paczyński, B. 1983, *ApJ*, 267, 315
- Ravenhall, D. G., & Pethick, C. J. 1994, *ApJ*, 424, 846
- Sazonov, S., & Sunyaev, R. 1996, *IAU Circ.*, 6291
- Shafter, A. W. 1992, *ApJ*, 394, 268
- Strickman, M. S. 1996, *ApJ*, 464, L131
- Sturmer, S. J., & Dermer, C. D. 1996 *ApJ*, 465, L31
- Swank, J. 1996, *IAU Circ.*, 6291
- Taam, R. E. 1982, *ApJ*, 258, 761
- Taam, R. E., & Picklum, R. E. 1979, *ApJ*, 233, 327
- Taam, R. E., Woosley, S. E., Weaver, T. A., & Lamb, D. Q. 1993, *ApJ*, 413, 324

Timmes, F. X., Woosley, S. E., & Weaver, T. A. 1996, *ApJ*, 457, 834

Van Wormer, L., Görres, J., Iliadis, C., Wiescher, M., & Thielemann, F.-K. 1994, *ApJ*, 432, 326

Wallace, R. K., & Woosley, S. E. 1981, *ApJS*, 43, 389

Wang, Y.-M. 1996, *ApJ*, 465, L111

Webbink, R. F., Rappaport, S., & Savonije, G. 1983, *ApJ*, 270, 678

Yakovlev, D. G., & Urpin, V. A. 1980, *AZh*, 57, 526

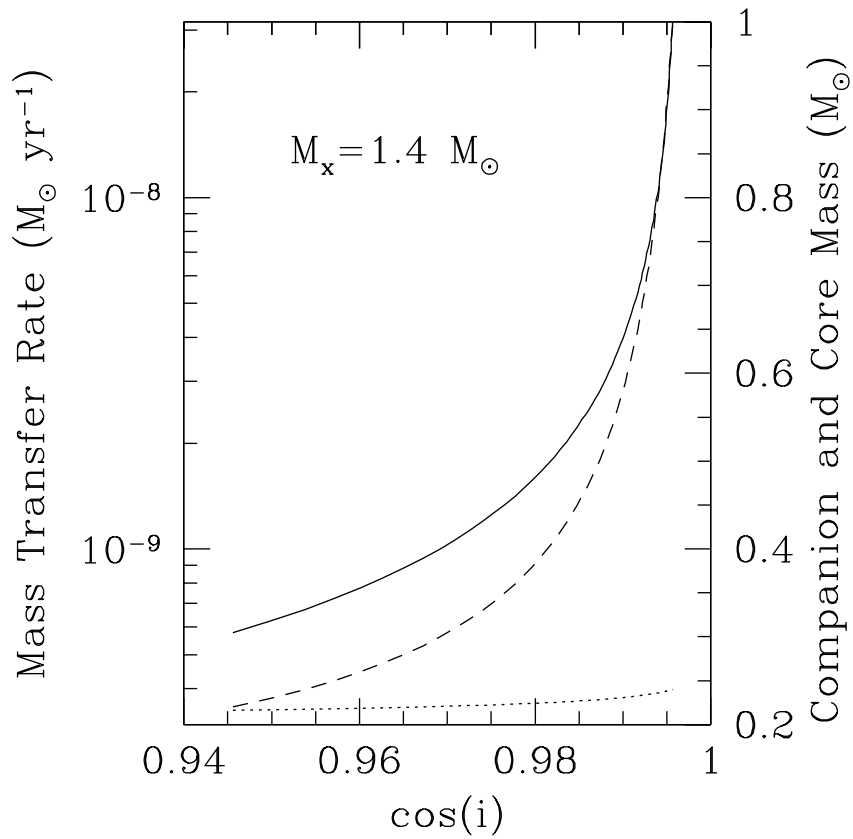


Fig. 1.— The companion mass and mass transfer rates as a function of inclination angle for $M_x = 1.4M_{\odot}$. For the orbital parameters of Finger et al. (1996), we show the red giant companion mass (dashed line) and inferred mass transfer rate (solid line) as a function of $\cos i$. There are no Roche-lobe filling solutions for $i > 18$ degrees if $M_x = 1.4M_{\odot}$.

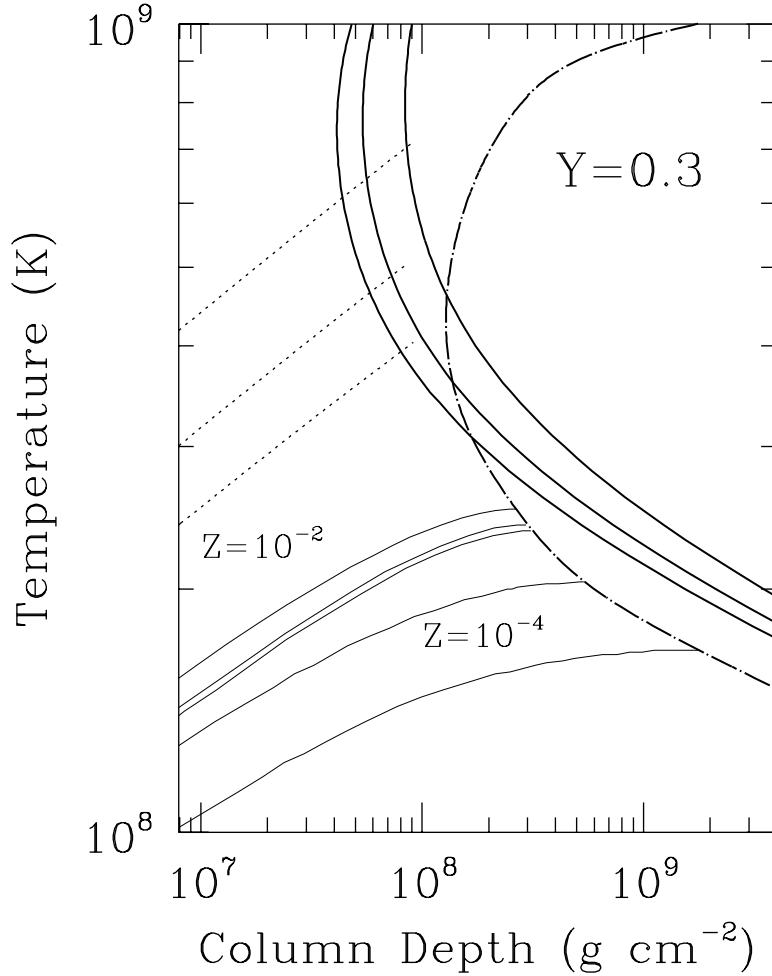


Fig. 2.— Helium ignition for hydrogen-rich accretion ($Y = 0.3$) at accretion rates appropriate for this source for a $1.4M_{\odot}$, $R = 10$ km neutron star. The heavy solid lines show the helium depletion curves for $\dot{m}_4 = 3, 7.5$, and 30 . The heavy dot-dashed curve is the helium ignition curve. The top three thin solid curves are settling solutions for $Z_{\text{CNO}} = 0.01$ and $\dot{m}_4 = 3, 7.5$, and 30 , while the bottom two are for $Z_{\text{CNO}} = 10^{-4}$ and $\dot{m}_4 = 7.5$ and 30 . The three dashed lines are the envelope structure if the burning were in steady-state for these three \dot{m} 's.

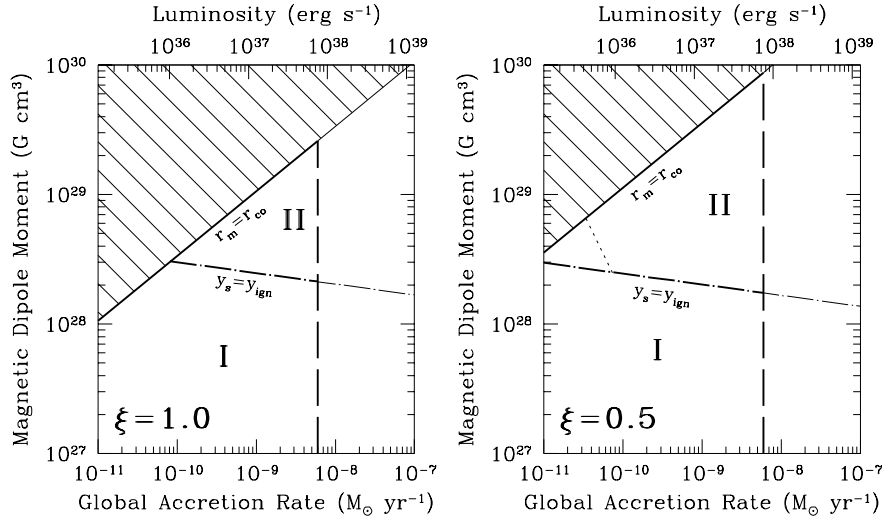


Fig. 3.— A graphical summary of the burning behavior parameterized by the dipole magnetic moment μ and the global accretion rate \dot{M} . The left plot is for $\xi = 1.0$; the right, for $\xi = 0.5$ (cf. equations [1] and [10]). We assume for simplicity that no higher-order multipole moments are present. In the shaded region the propeller effect stops accretion (i.e., $r_m > r_{co}$). For the region beneath the dot-dashed line labeled $y_s = y_{\text{ign}}$, spreading occurs above the ignition column depth $y_{\text{ign}} \approx 2 \times 10^8 \text{ g cm}^{-2}$. The vertical dashed line indicates the critical accretion rate, $m_{\text{crit}} = 3 \times 10^4 \text{ g cm}^{-2} \text{ s}^{-1}$, for spherically symmetric accretion. In region I, the burning is unstable regardless of polar cap size. For region II, the accreted material is magnetically confined at the ignition column density; our ignorance of the polar cap size prohibits us from indicating where the burning is unstable. In the right-hand plot we show with a dotted line where unstable burning begins if the accreted material is confined to a polar cap of area given by equation (10). Nuclear burning is unstable in the region to the left of this line.